Finite Volume Solution of Non-Newtonian Casson Fluid Flow in A Square Cavity | Research Article

S. Mehmood[1],*, M. Nawaz[1] and A. Ali[2]

[1] *Department of Applied Mathematics and Statistics, Institute of Space Technology, Islamabad, Pakistan*
[2] *Department of Space Science, Institute of Space Technology, Islamabad, Pakistan*
*****Corresponding author:** sumaira_61554@outlook.com

Abstract. A two dimensional unsteady flow of non-Newtonian fluid in a square cavity is investigated numerically by using finite volume method based on staggered grids. The discretized equations are integrated by using second order Adams-Bashforth time advancement scheme togather with pressure correction approach. Error history for velocities and pressure are recorded for high Reynolds number when grid resolution is 128×128. The results are also compared with already published work for special case. An excellent agreement is observed. The behavior of velocity components are studied for different values of non-Newtonian parameter β, the Casson fluid parameter.

Keywords. Finite volume method; Casson fluid; Driven cavity flow; Staggered grid; Pressure Poisson equation; Thomas algorithms; Adam Bashfort

MSC. 76A05

Received: January 29, 2018   **Accepted:** April 6, 2018

1. Introduction

Many fluids at industry and engineering are non-Newtonian in nature. Different constitutive equations for non-Newtonian fluids [12–14] have been proposed. Constitutive equations for Casson fluid [21] are one of them. Casson fluid behaves like an elastic solid. Such kind of fluid

exhibits simultaneous effects including shear thinning, yield stress and high shear viscosity [2]. Several investigators have studied the flow of Casson fluid over different geometries. For example, Mustafa *et al.* [21] studied boundary layer Casson fluid flow induced by the impulsive motion of flat plate. Analytic solution for magneto hydrodynamic flow of Casson fluid was computed by Nadeem *et al.* [22]. Eldabe and Salwa [9] analyzed heat transfer characteristics in the flow of Casson fluid between two rotating spheres.

The pioneering work on the flow of Newtonian fluid in a square cavity is investigated by Ghia *et al.* [10]. This remarkable investigation, which is most referred source of results on the lid driven cavity flow. Several studies on the flow of Newtonian fluid in a square cavity have been conducted and almost, all studies have been validated by comparing the results with the results computed by Ghia *et al.* [10]. For moderate Reynolds number, the boundary element analysis was performed by Aydin and Fenner [3] to study the flow of Newtonian fluid in the cavity. Barragy and Carey [4] used finite element method to solve the problem describing the flow in a square cavity. They investigated vortex flow features and minimized the influence of the corner singularities through graded meshing. The steady laminar flow for large Reynolds number was discussed by Batchelor [5]. Benjamin and Denny [6] studied the effect of large Reynolds number on the convergence of numerical solution for flow in a cavity. Gupta and Manohar [11] discussed the accuracy of numerical solutions of viscous flow in a cavity. Simulations for the flow in a cavity using lattice Boltzmann method are carried out by Hou *et al.* [15]. Li *et al.* [18] developed a compact fourth order finite difference scheme for steady incompressible Navier-Stokes equations. Liao [19] used higher resolution scheme for two-dimensional steady flow in a square cavity. Nishida and Satofuka [23] derived higher order solutions for two dimensional flow induced by the motion of lid moving with constant velocity. Peng *et al.* [24] studied transition in two-dimensional flow in a cavity. Weinan and Liu [28] addressed the issues related to vortices boundary conditions for finite difference schemes. Botella and Peyret [7] computed the numerical solution of two dimensional Navier-Stokes equations describing the lid driven cavity flow by the Chebyshev collocated method. They also validated their results by comparing them with the results obtained by Ghia *et al.* [10]. Kumar *et al.* [17] presented the numerical solution for two-dimensional flow using multigrid scheme in conjunction with finite volume SIMPLE algorithm for different values of Reynolds number and validated their results by comparing with the results of Ghia *et al.* [10]. Darwish *et al.* [8] implemented and tested a new numerical algorithm similar to SIMPLE algorithm for two-dimensional Navier-Stokes equations. They validated their algorithm by solving some test problems including lid driven cavity problem. Kim *et al.* [16] implemented collocated finite volume scheme for two-dimensional Navier-Stokes equations and tested the algorithm by solving benchmark problems including lid driven cavity flow problem and the problem of natural convection between two eccentric cylinders. Three dimensional lid driven cavity flow was simulated by Albensoeder and Kuhlmann [1] using numerical algorithm with time advancement integration of Adams-Bashforth backward Euler scheme. Marchi *et al.* [20] performed simulations for cavity flow with high order resolution.

Sahin and Owens [25] introduced a novel finite volume method for cavity flow taking high Reynolds number. Numerical study regarding three-dimensional flow in a cubic cavity was conducted by Takami and Kuwahara [26]. Numerical solution for incompressible flow in a square cavity was computed using method of discrete singular convolution by Wan *et al*. [27].

Literature survey reveals that the majority of investigations with respect to the cavity flows examine Newtonian fluid flow a square cavity. No study with respect to Casson fluid (non-Newtonian) flow in a cavity is examined yet. This paper is an attempt in this direction. This manuscript is organized in six sections. In Section 2, mathematical formulation of governing equations are presented. In Section 3, the finite volume method is presented. Discretization procedure is given in Section 4. Section 5 is dedicated for results and discussion. Concluding remarks are given in Section 6.

2. Mathematical Description

Initially, the non-Newtonian fluid (the Casson fluid) and the lid of the cavity are rest. Suddenly the lid of the cavity is set into motion with constant speed U in the positive x-direction. Two dimensional unsteady flow occurs with no thermal changes. During the flow physical properties of the fluid remain constant. No slip assumption is valid. The coordinate configuration and physical model is shown in Figure 1.
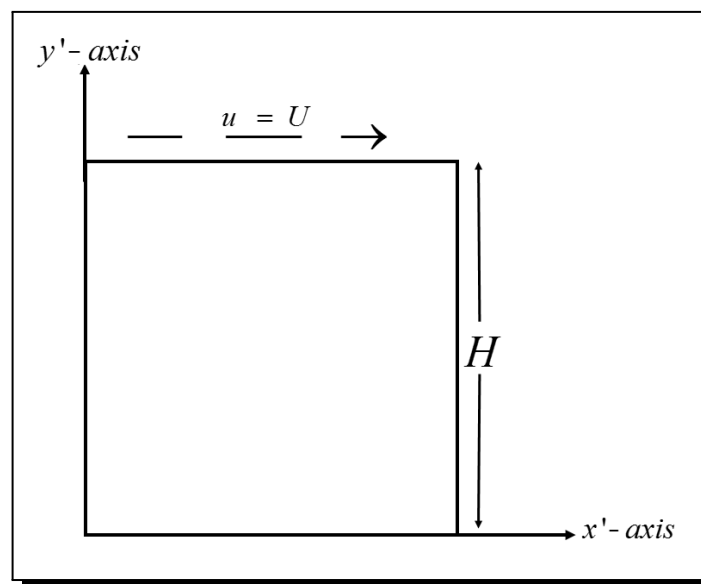

Figure 1. Geometry of physical happening and coordinate axes.

Continuity and momentum equations, for incompressible flow of Casson fluid are given

$$\nabla \cdot \boldsymbol{V} = 0, \tag{2.1}$$

$$\rho \frac{dV}{dt} = -\nabla p + \operatorname{div} \tau. \tag{2.2}$$

In which ρ is the density, $\boldsymbol{V}$ is the velocity of the fluid, $d/dt = \partial/\partial t + \boldsymbol{V} \cdot \nabla$, is the material derivative, p is the pressure and τ is the stress tensor for Casson fluid [12–14] and is defined by

$$\tau_{ij} = \mu_B + \left[\left(\frac{P_y}{\sqrt{2\pi_c}} \right)^{\frac{1}{n}} \right]^n 2e_{ij}, \tag{2.3}$$

where e_{ij} is the deformation rate, μ_B is the dynamic viscosity and π_c is the critical value of $\pi = e_{ij}e_{ij}$. It is important to mention that the coming analysis will be perform $n = 1$. For incompressible flow, τ given in eq. (2.3) can be written as

$$\tau = -pI + \left(1 + \frac{1}{\beta} \right) \left[\operatorname{grad} \boldsymbol{V} + (\operatorname{grad} \boldsymbol{V})^t \right], \tag{2.4}$$

where $\beta = \mu_B \sqrt{2\pi_c}/P_y$, is the Casson fluid parameter. Here it is important to mention that if $\beta \to \infty$, eq. (2.4) reduces to the case of Newtonian fluid.

Unsteady two-dimensional flow is characterized by the velocity field

$$V' = [u(x', y', t), v(x', y', t), 0]. \tag{2.5}$$

Using the eq. (2.5) in eqs. (2.1)-(2.3), we get

$$\left(\frac{\partial u'}{\partial x'} \right) + \left(\frac{\partial v'}{\partial y'} \right) = 0, \tag{2.6}$$

$$\left(\frac{\partial u'}{\partial t'} \right) + u' \left(\frac{\partial u'}{\partial x'} \right) + v' \left(\frac{\partial v'}{\partial y'} \right) = -\left(\frac{1}{\rho} \right) \left(\frac{\partial p'}{\partial x'} \right) + v \left(1 + \frac{1}{\beta} \right) \left(\frac{\partial^2 u'}{\partial x'^2} \right) + \left(\frac{\partial^2 u'}{\partial y'^2} \right), \tag{2.7}$$

$$\left(\frac{\partial v'}{\partial t'} \right) + u' \left(\frac{\partial v'}{\partial x'} \right) + v' \left(\frac{\partial v'}{\partial y'} \right) = -\left(\frac{1}{\rho} \right) \left(\frac{\partial p'}{\partial y'} \right) + v \left(1 + \frac{1}{\beta} \right) \left(\frac{\partial^2 v'}{\partial x'^2} \right) + \left(\frac{\partial^2 v'}{\partial y'^2} \right). \tag{2.8}$$

Here $v = \mu/\rho$ is the kinematic viscosity.

Initial and boundary conditions are

$$u(x', y', 0) = 0, v(x', y', 0) = 0, \quad t < 0, \tag{2.9}$$

$$\left\{ \begin{array}{ll} u(x', 0, t) = U, \ v(x', 0, t) = 0, & 0 < x' < H, \ t > 0, \\ u(x', H, t) = 0, \ v(x', H, t) = 0, & 0 \le x' \le H, \ t > 0, \\ u(0, y', t) = 0, \ v(0, y', t) = 0, & 0 \le y' \le H, \ t > 0, \\ u(H, y', t) = 0, \ v(H, y', t) = 0, & 0 \le y' \le H, \ t > 0. \end{array} \right\} \tag{2.10}$$

where H is the dimension of the square cavity.

Following change of variables converts eqs. (2.6)-(2.10)

$$u = \frac{u'}{U}, \ v = \frac{v'}{U}, \ x = \frac{x'}{H}, \ y = \frac{y'}{H}, \ \tau = \frac{tU}{H}, \ p = \frac{p'}{\rho U^2}, \ Re = \frac{UH}{v}.$$

Into following non-dimensional conservative initial boundary value problem

$$\frac{\partial u}{\partial x} + \frac{\partial v}{\partial y} = 0, \tag{2.11}$$

$$\frac{\partial u}{\partial \tau} + \frac{\partial}{\partial x}(u^2) + \frac{\partial}{\partial y}(uv) = -\frac{\partial p}{\partial x} + \frac{1}{Re} \left(1 + \frac{1}{\beta} \right) \left(\frac{\partial}{\partial x} \left(\frac{\partial u}{\partial x} \right) + \frac{\partial}{\partial y} \left(\frac{\partial u}{\partial y} \right) \right), \tag{2.12}$$

$$\frac{\partial v}{\partial \tau} + \frac{\partial}{\partial x}(uv) + \frac{\partial}{\partial y}(v^2) = -\frac{\partial p}{\partial y} + \frac{1}{Re}\left(1 + \frac{1}{\beta}\right)\left(\frac{\partial}{\partial x}\left(\frac{\partial v}{\partial x}\right) + \frac{\partial}{\partial y}\left(\frac{\partial v}{\partial y}\right)\right),\tag{2.13}$$

$$\begin{cases} u(x,y,0)=0,\ v(x,y,0)=0, & \tau<0, \\ u(x,0,\tau)=0,\ v(x,0,\tau)=0, & 0\le x\le 1,\ \ \tau>0, \\ u(x,1,\tau)=1,\ v(x,1,\tau)=0, & 0\le x\le 1,\ \ \tau>0, \\ u(0,y,\tau)=0,\ v(0,y,\tau)=0, & 0\le y\le 1,\ \ \tau>0, \\ u(1,y,\tau)=0,\ v(1,y,\tau)=0, & 0\le y\le 1,\ \ \tau>0. \end{cases}\tag{2.14}$$

Here $Re = UH/v$ is the Reynolds number. It is important to note that as $\beta \to \infty$ the initial boundary value problem given in eqs. (2.11)-(2.14) reduces to the Newtonian case.

3. Finite Volume Method

Two dimensional initial boundary value problems given in eqs. (2.11)-(2.14) are discretized by the finite volume approach through the staggered grid. Control volumes for u-velocity, v-velocity and p-pressure are given in Figure 2, where u-velocity is located midway on vertical faces of the control volume and v-velocity is stored at midway on horizontal faces of the control volume. Pressure-velocity coupling approach (pressure correction method) is applied.
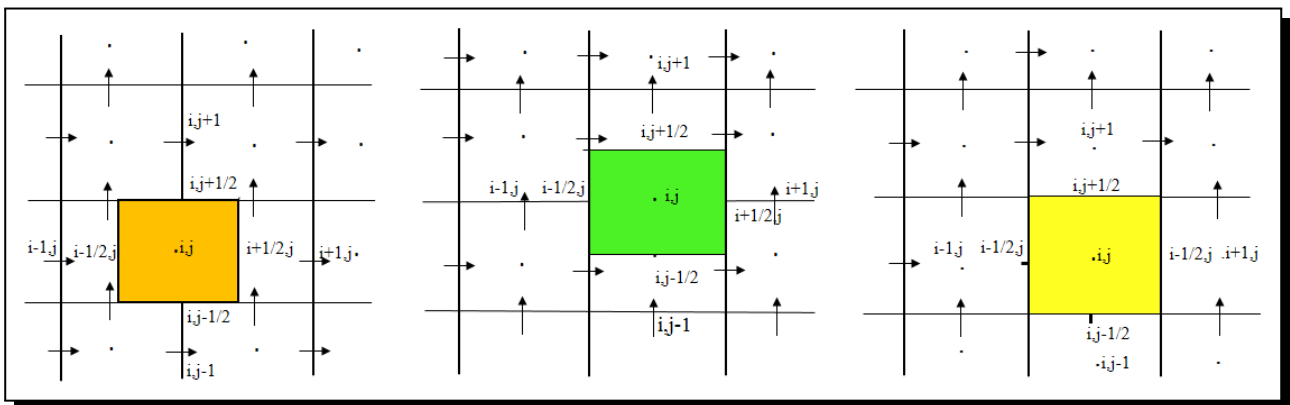

Figure 2. Control volumes for staggered grid for velocities u (left), v (center) and pressure (right).

4. Discretization Procedure

Continuity equation

$$\frac{u_{i+1,j} - u_{i,j}}{\Delta x} + O(\Delta x^2) + \frac{v_{i,j+1} - v_{i,j}}{\Delta y} + O(\Delta y^2) = 0.\tag{4.1}$$

Correct the intermediate velocity values with the newly established pressure gradients.

$$un^{+1} = u^* - \Delta t \nabla p,\quad vn^{+1} = v^* - \Delta t \nabla p.$$

The terms u^* and v^* are intermediate values.

$$u_{i+1,j}^{n+1} = u_{i+1,j}^* - \Delta t\frac{p_{i+1,j} - p_{i,j}}{\Delta x},\quad u_{i,j}^{n+1} = u_{i,j}^* - \Delta t\frac{p_{i,j} - p_{i-1,j}}{\Delta x},\tag{4.2}$$

$$v_{i,j+1}^{n+1} = v_{i,j+1}^* - \Delta t \frac{p_{i,j+1} - p_{i,j}}{\Delta y}, \quad v_{i,j}^{n+1} = v_{i,j}^* - \Delta t \frac{p_{i,j} - p_{i,j-1}}{\Delta y}. \tag{4.3}$$

Using the eqs. (4.2), (4.3) in eq. (4.1), one obtains

$$A_p P_p + \sum_l A_l P_l = Q_{i,j}, \tag{4.4}$$

where

$$A_N = A_S = \frac{\Delta x}{\Delta y}, \qquad A_E = A_W = \frac{\Delta y}{\Delta x},$$

$$A_P = -\sum_l A_l = -2 \left(\frac{\Delta x}{\Delta y} + \frac{\Delta y}{\Delta x} \right),$$

$$Q_{i,j} = \frac{1}{\Delta \tau} ((u_{i+1,j}^* + u_{i,j}^*) \Delta y + (v_{i,j+1}^* - v_{i,j}^*) \Delta x).$$

Here u^* and v^* are intermediate velocity values.

x-momentum equation

$$\frac{\partial u}{\partial \tau} = \frac{u_{i,j}^{n+1} - u_{i,j}^n}{\Delta \tau} + O(\Delta \tau),$$

$$\frac{\partial}{\partial x}(u^2) = \frac{u_e^2 - u_w^2}{\Delta x} + O(\Delta x^2), \quad u_e^2 = \frac{1}{4}(u_{i,j} + u_{i+1,j})^2, \ u_w^2 = \frac{1}{4}(u_{i-1,j} + u_{i,j})^2,$$

$$\frac{\partial(uv)}{\partial y} = \frac{(uv)_n - (uv)_s}{\Delta y} + O(\Delta y^2),$$

$$u_n = \frac{1}{2}(u_{i,j} + u_{i,j+1}), \ u_s = \frac{1}{2}(u_{i,j-1} + u_{i,j}),$$

$$v_n = \frac{1}{2}(v_{i-1,j+1} + v_{i,j+1}),$$

$$v_s = \frac{1}{2}(v_{i-1,j} + v_{i,j}),$$

$$\frac{\partial}{\partial x}\left(\frac{\partial u}{\partial x}\right) = \frac{\left(\frac{\partial u}{\partial x}\right)_e - \left(\frac{\partial u}{\partial x}\right)_w}{\Delta x} + O(\Delta x^2),$$

$$\left(\frac{\partial u}{\partial x}\right)_e = \frac{(u_{i+1,j} - u_{i,j})}{(\Delta x)}, \quad \left(\frac{\partial u}{\partial x}\right)_w = \frac{u_{i,j} - u_{i-1,j}}{(\Delta x)},$$

$$\left(\frac{\partial}{\partial y}\right)\left(\frac{\partial u}{\partial y}\right) = \frac{\left(\frac{\partial u}{\partial y}\right)_n - \left(\frac{\partial u}{\partial y}\right)_s}{(\Delta y)} + O(\Delta y^2), \quad \left(\frac{\partial u}{\partial y}\right)_n = \frac{u_{i,j+1} - u_{i,j}}{(\Delta y)},$$

$$\left(\frac{\partial u}{\partial y}\right)_s = \frac{u_{i,j} - u_{i,j-1}}{(\Delta y)}.$$

y-momentum equation

$$\frac{\partial v}{\partial \tau} = \frac{v_{i,j}^{n+1} - v_{i,j}^n}{\Delta \tau} + O(\Delta \tau),$$

$$\frac{\partial}{\partial y}(v^2) = \frac{v_n^2 - v_s^2}{\Delta y} + O(\Delta y^2), \quad v_n^2 = \frac{1}{4}(v_{i,j} + v_{i,j+1})^2, \quad v_s^2 = \frac{1}{4}(v_{i,j-1} + v_{i,j})^2,$$

$$\frac{\partial (uv)}{\partial x} = \frac{(uv)_e - (uv)_w}{\Delta x} + O(\Delta x^2),$$

$$u_e = \frac{1}{2}(u_{i,j} + u_{i,j-1}), \quad u_w = \frac{1}{2}(u_{i-1,j} + u_{i-1,j+1}),$$

$$v_e = \frac{1}{2}(v_{i,j} + v_{i+1,j}), \quad v_w = \frac{1}{2}(v_{i-1,j} + v_{i,j}),$$

$$\frac{\partial}{\partial x}\left(\frac{\partial v}{\partial x}\right) = \frac{\left(\frac{\partial v}{\partial x}\right)_e - \left(\frac{\partial v}{\partial x}\right)_w}{\Delta x} + O(\Delta x^2),$$

$$\left(\frac{\partial v}{\partial x}\right)_e = \frac{(v_{i+1,j} - v_{i,j})}{(\Delta x)}, \quad \left(\frac{\partial v}{\partial x}\right)_w = \frac{v_{i,j} - v_{i-1,j}}{(\Delta x)},$$

$$\left(\frac{\partial}{\partial y}\right)\left(\frac{\partial v}{\partial y}\right) = \frac{\left(\frac{\partial v}{\partial y}\right)_n - \left(\frac{\partial v}{\partial y}\right)_s}{(\Delta y)} + O(\Delta y^2), \quad \left(\frac{\partial v}{\partial y}\right)_n = \frac{v_{i,j+1} - v_{i,j}}{(\Delta y)}, \quad \left(\frac{\partial v}{\partial y}\right)_s = \frac{v_{i,j} - v_{i,j-1}}{(\Delta y)}.$$

Boundary conditions

No slip assumption gives rise the boundary conditions which are given by eqs. (2.14). The discretized form of boundary conditions are

$u = v = 0,$	$v_{1,j} = -v_{2,j} u_{2,j} = 0$	at west/left wall
$u = v = 0,$	$v_{n,j} = -v_{n-1,j} u_{n,j} = 0$	at east/right wall
$u = v = 0,$	$v_{i,2} = 0, \; u_{i,1} = -u_{i,2}$	at south/bottom wall
$u = 1, \; v = 0,$	$v_{i,n} = 0, \; u_{i,n} = 2 - u_{i,n-1}$	at north/top wall

5. Results and Discussions

Errors convergence history on grid size 128×128 for velocities and pressure are plotted in Figure 3. The L_2 norm of the change solution of u-velocity and p-pressure is plotted against number of iteration using 0.000125 time step size. The large time step values require large solution time to converge. Figure 4 represents that the u-velocity profile along a horizontal line $y = (1/2)$ passing through the centre of the cavity with different value of Casson fluid parameter (β), Reynolds number (Re) 1000 and grid size 128×128. This figure shows that $u(x, 0.5)$ increases in the region $0 < y < 0.95$ whereas it decreases in the rest of the region. However, $u(x, 0.5)$ for Newtonian fluid ($\beta \to \infty$) is higher than in the regions $0 < y < 0.19$ and $0.92 < y \le 1$ while in case of Non-Newtonian ($\beta \to \infty$) it decreases in the region $0.19 < y < 0.9$. Figure 5 shows the variation of vertical velocity along horizontal $x = (1/2)$ for different value of

Casson fluid parameter (β), Reynolds number (Re) 1000 and grid size 128×128. The present results are validated by the comparing with already published work of Ghia *et al*. [10] when Reynolds number $Re = 1000$. This comparison is recorded in Tables 1 and 2. Table 1. contains the values of u-velocity when $x = (1/2)$ at 128×128 grid resolution. Whereas, Table 2 contains the values of v-velocity when $y = (1/2)$ at grid resolution 128×128. These tables shows a good agreement between the present results and the already published work of Ghia *et al*. [10]. The streamlines are displayed in Figure 6 when $\beta = 0.93$ and $Re = 1000$ for 128×128 grid resolution. In contrast to the results obtained in the stream function-vorticity formulation, the vortices are noted in the bottom corners of the cavity. u-velocity contours are given in Figure 7 and Figure 8 whereas shows color map graph of u-velocity contours when Reynolds number $Re = 1000$ and the Casson fluid parameter $\beta = 0.93$. v-velocity contours are sketched in Figure 9 Similarly, Figure 10 show color map graph of v-velocity contours when $Re = 1000$ and $\beta = 0.93$. Extreme values of velocity components are recorded in Table 3 when Reynolds number $Re = 1000$ at different grid resolutions both for Newtonian and non-Newtonian cases.

Table 1. Results validation when $Re = 1000$ and $\beta \to \infty$.

	FVM	Ghia *et al*. [10]
Y	129×129	129×129
1.0000	1.0000	1.0000
0.9766	0.6539	0.9766
0.9688	0.5723	0.9688
0.9609	0.5109	0.9609
0.9531	0.4653	0.9531
0.8516	0.3313	0.8516
0.7344	0.1847	0.7344
0.6172	0.05738	0.6172
0.5000	−0.06016	0.5000
0.4531	−0.1017	0.4531
0.2813	−0.2754	0.2813
0.1719	−0.3805	0.1719
0.1016	−0.2911	0.1016
0.0703	−0.2278	0.0703
0.0625	−0.2020	0.0625
0.0547	−0.1801	0.0547
0.0000	0.0000	0.0000

Table 2. Results validation when $Re = 1000$ and $\beta \rightarrow \infty$.

	FVM	Ghia *et al.* [10]
x	129×129	129×129
1.0000	0.0000	0.0000
0.9688	−0.2131	−0.21388
0.9609	−0.2756	−0.27669
0.9531	−0.3370	−0.33714
0.9453	−0.3912	−0.39188
0.9063	−0.5145	−0.51550
0.8594	−0.4263	−0.42665
0.8047	−0.3191	−0.31966
0.5000	0.02520	0.02526
0.2344	0.3220	0.32235
0.2266	0.3303	0.33075
0.1563	0.3711	0.37095
0.0938	0.3262	0.32627
0.0781	0.3032	0.30353
0.0703	0.2910	0.29012
0.0625	0.2742	0.27485
0.0000	0.0000	0.0000

Table 3. Extreme values of velocity components under the influence of β and Re.

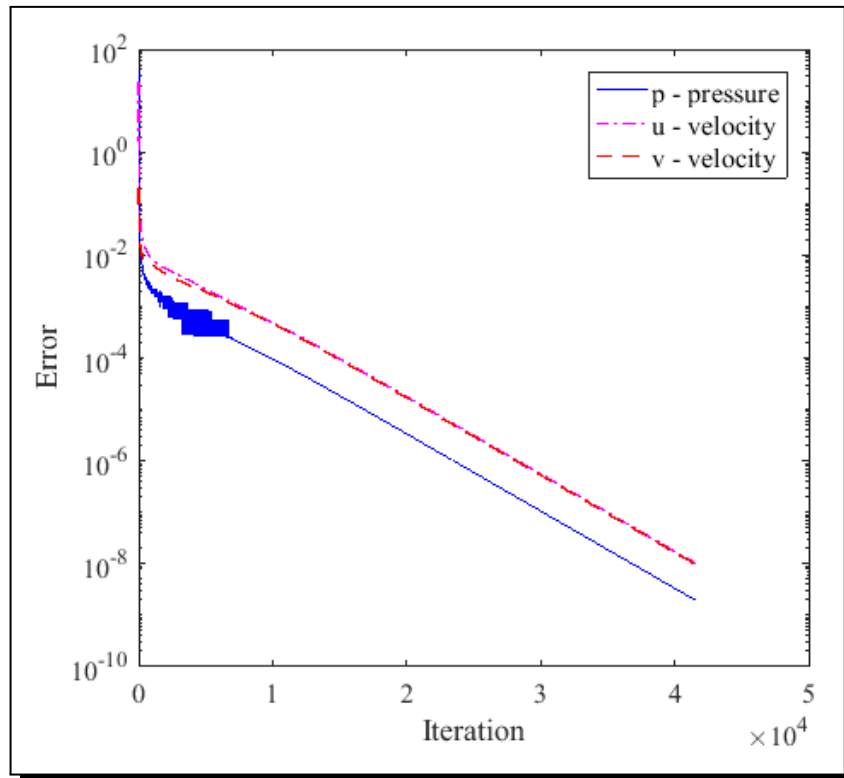| Casson fluid parameter	Reynolds number	Velocities			
B	Re	$u_{\min}$	$u_{\max}$	$v_{\min}$	$v_{\max}$
0.47 (Non-Newtonian case)	1000	−0.3226	1.0000	−0.6284	0.3476
0.93 (Non-Newtonian case)	1000	−0.3477	1.0000	−0.6473	0.3821
∞ (Newtonian case)	1000	−0.3844	1.0000	−0.6681	0.4516
0.93	100	−0.2184	1.0000	−0.4642	0.3443
0.93	500	−0.3033	1.0000	−0.6116	0.3281
0.93	1000	−0.3477	1.0000	−0.6473	0.3821

Figure 3. Error history when $Re = 1000$, $\beta = 0.93$ on 128×128 grids.
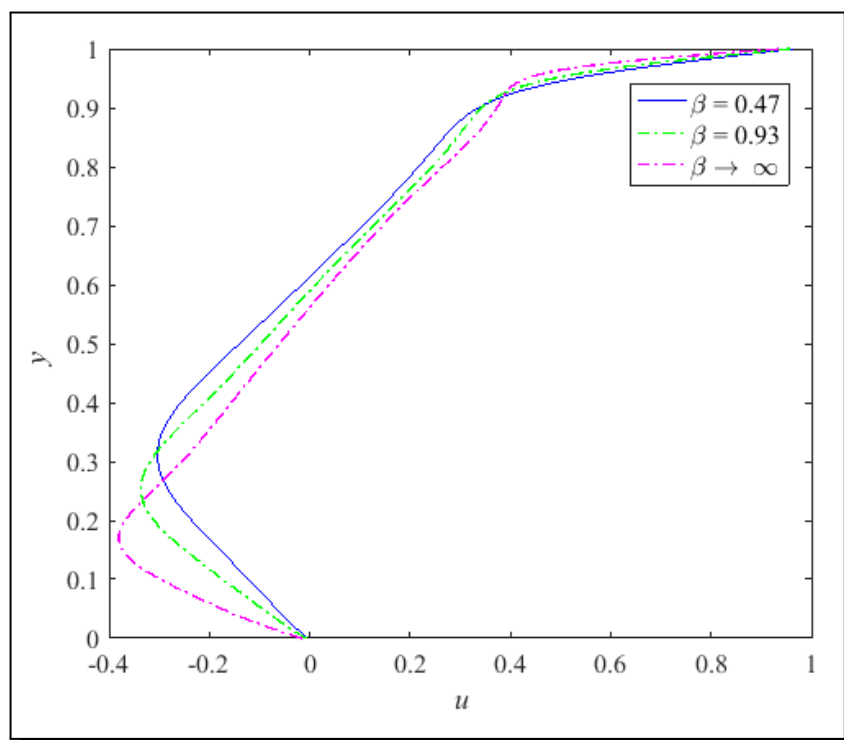

Figure 4. Behavior of $u(x = 0.5, y)$ under the variation of Casson fluid parameter β.
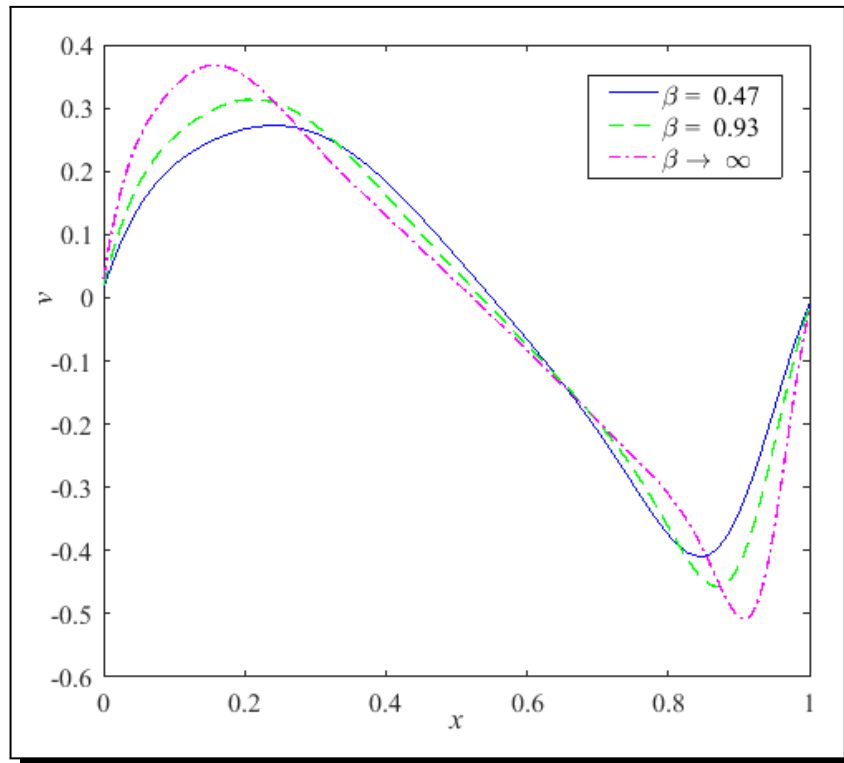
Figure 5. Behaviour of $v(x, y = 0.5)$ for various values of Casson fluid parameter β.
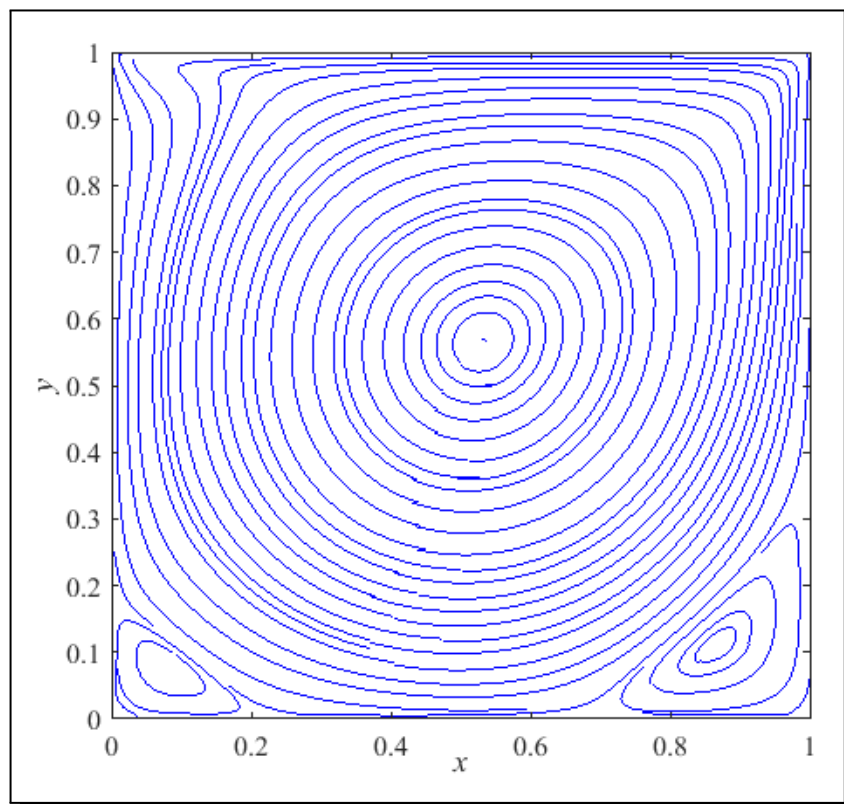

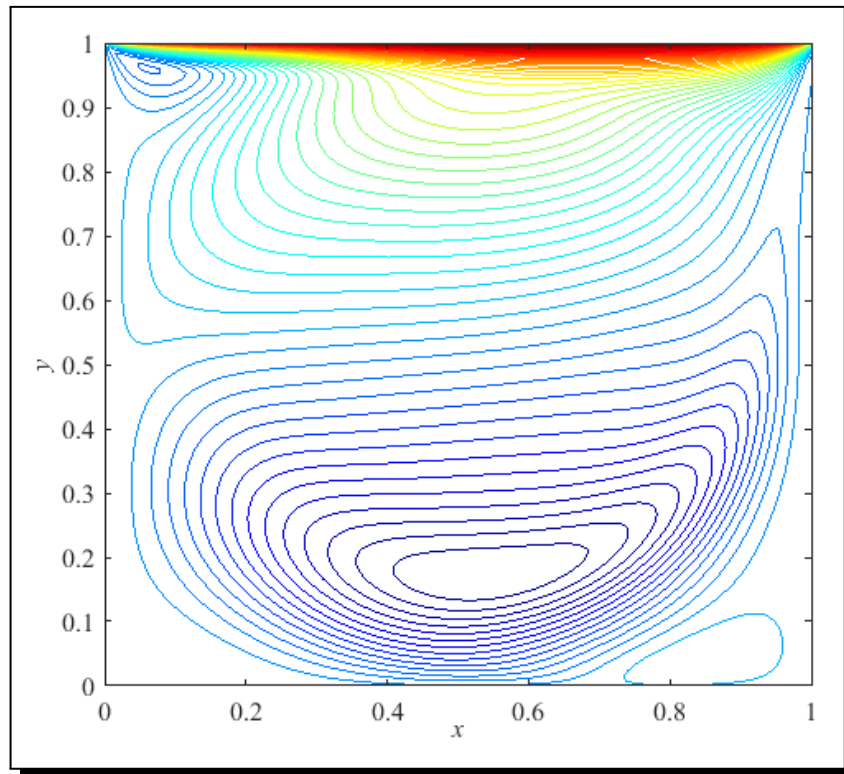**Figure 6.** Streamlines when $\beta = 0.93$, $Re = 1000$ on 128×128 grids.

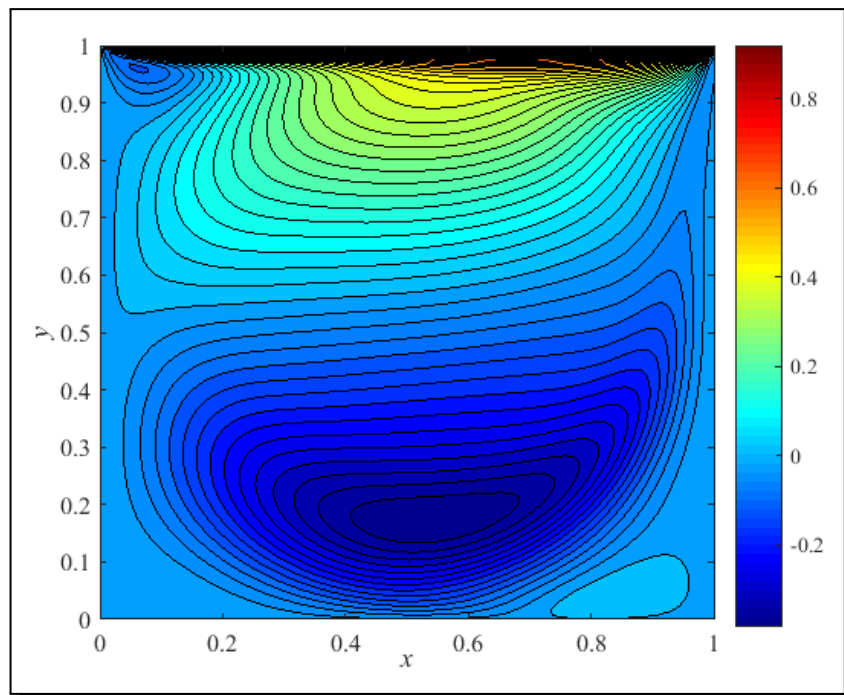**Figure 7.** u-velocity contours when $\beta = 0.93$ and $Re = 1000$.

Figure 8. Color map graph for u-velocity contours when $\beta = 0.93$ and $Re = 1000$.

Figure 9. v-velocity contours when $\beta = 0.93$ and $Re = 1000$.

Figure 10. Color map graph for v-velocity contours when $\beta = 0.93$ and $Re = 1000$.
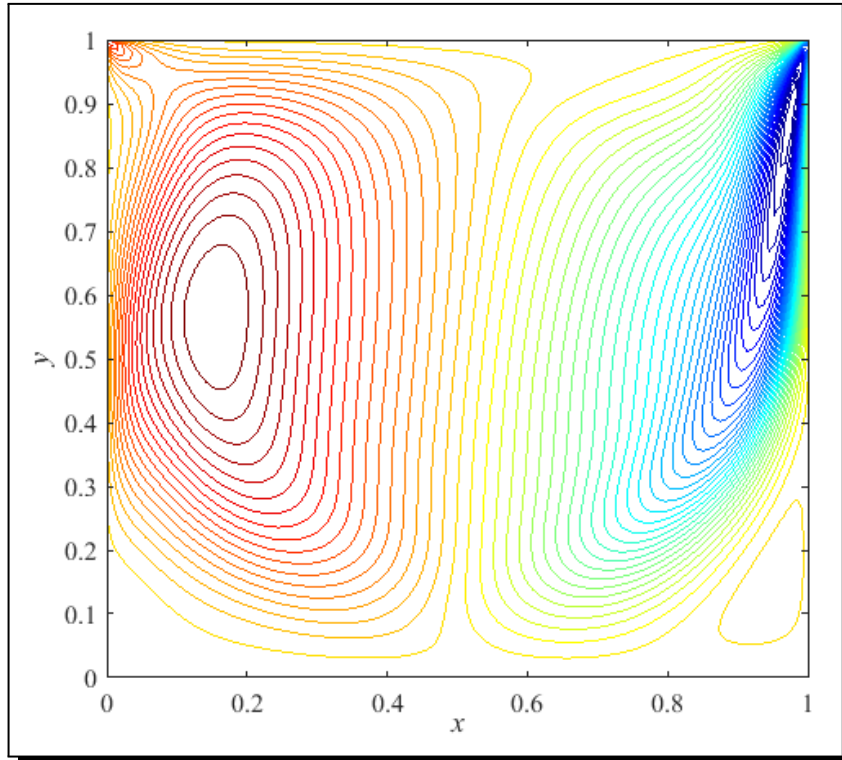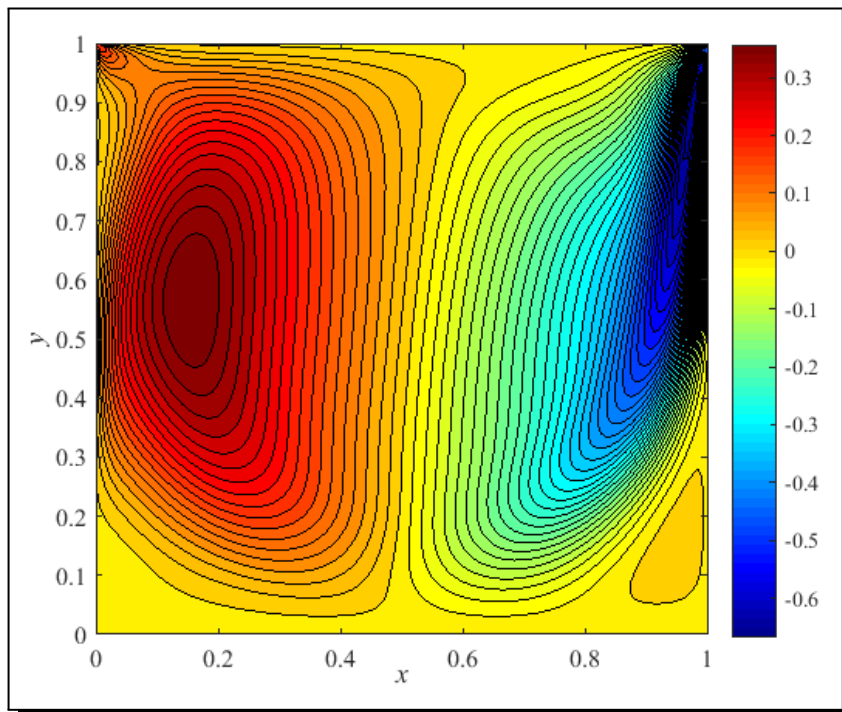
6. Concluding Remarks

Unsteady two-dimensional flow of problem Casson fluid in the square cavity are solved numerically by finite volume approach with number of solvers (ADI with SOR) for linear system of algebraic equations. For time advancement, second order Adams-Bashforth integration scheme is used. The pressure Poisson equation is solved in conjunction with successive over relaxation (SOR) method with the computational tolerance 10×8. Convergence of unknowns (velocities and pressure) ensured through series of simulations for high values of Reynolds number and $\beta = 0.93$ on 128×128 grids. Behaviour of streamlines, velocity and extreme values of velocities under different values of Reynolds number (Re) and Casson fluid parameter (β) is recorded. The present results are also validated through the comparison with Ghia *et al*. [10]. Which is special case of the present study. The behavior of streamlines also compared with streamlines obtained by the method of vorticity stream function formulation. This comparison shows that the finite volume method for velocity pressure coupling is capable of capturing vortices.

Competing Interests

The author declares that he has no competing interests.

Authors' Contributions

The author wrote, read and approved the final manuscript.

References

[1] S. Albensoeder and H.C. Kuhlmann, Accurate three-dimensional lid-driven cavity flow, *Journal of Computational Physics* **206** (2) (2005), 536 – 558.

[2] L. Animasaun, E.A. Adebile and A.I. Fagbade, Casson fluid flow with variable thermo-physical property along exponentially stretching sheet with suction and exponentially decaying internal heat generation using the homotopy analysis method, *Journal of the Nigerian Mathematical Society* **35** (2016), 1 – 17.

[3] M. Aydin and R.T. Fenner, Boundary element analysis of driven cavity flow for low and moderate Reynolds number, *International Journal for Numerical Methods in Fluids* **37** (1) (2001), 45 – 64.

[4] E. Barragy and G.F. Carey, Stream function-vorticity driven cavity solution using p finite elements, *Computers and Fluids* **26** (5) (1997), 453 – 468.

[5] G.K. Batchelor, On steady laminar flow with closed streamlines at large Reynolds number, *Journal of Fluid Mechanics* **1** (2) (1956), 177 – 190.

[6] A.S. Benjamin and V.E. Denny, On the convergence of numerical solutions for 2-D flows in a cavity at large Re, *Journal of Computational Physics* **33** (3) (1979), 340 – 358.

[7] O. Botella and R. Peyret, Benchmark spectral results on the lid-driven cavity flow *Computers and Fluids* **27** (4) (1998), 421 – 433.

[8] M. Darwish, I. Sraj and F. Moukalled, A coupled incompressible flow solver on structured grids, *Numerical Heat Transfer, Part B: Fundamentals* **52** (4) (2007), 353 – 371.

[9] N.T.M. Eldabe and M.G.E. Salwa, Heat transfer of MHD non-Newtonian Casson fluid flow between two rotating cylinders, *Journal of Physical Socity of Japan* **64** (1995), 41 – 64.

[10] U.K. Ghia, K.N. Ghia and C.T. Shin, High-Re solutions for incompressible flow using the Naiver-Stokes equations and multigrid method, *Journal of Computational Physics* **48** (3) (1982), 387 – 411.

[11] M.M. Gupta and R.P. Manohar, Boundary approximations and accuracy in viscous flow computations, *Journal of Computational Physics* **31** (2) (1979) 265 – 288.

[12] T. Hayat and M. Nawaz, Soret and Dufour effects on the mixed convection flow of a second grade fluid subject to Hall and ion-slip current, *International Journal for Numerical Methods in Fluids* **66** (9) (2011), 1073 – 1099.

[13] T. Hayat, M. Nawaz, M. Awais and S. Obaidat, Axisymmetric magneto hydrodynamic flow of Jeffrey fluid over a rotating disk, *International Journal for Numerical Methods in Fluids* **70** (6) (2012), 764 – 774.

[14] T. Hayat, M. Nawaz, S. Asghar and S. Mesloub, Thermal-diffusion and diffusion-thermo effects on axisymmetric flow of a second grade fluid, *International Journal of Heat and Mass Transfer* **54** (13-14) (2011), 3031 – 3041.

[15] S. Hou, Q. Zou, S. Chen, G. D. Doolen and A.C. Cogely, Simulation of cavity flow by the Lattice Boltzmann method, *Journal of Computational Physics* **118** (1995), 329 – 347.

[16] J. Kim, I.K. Park, H.K. Cho, Y.H. Yoon and J.J. Jeong, Collocated scheme on an unstructured mesh for two-phase flow analyses, *Proceeding of Korean National Society Spring Meeting* **40** (45) (2009), 659 – 650.

[17] D.S. Kumar, K.S. Kumar and M.D. Kumar, A fine grid solution for a lid-driven cavity flow using multigrid method *Engineering Applications of Computational Fluid Mechanics* **3** (3) (2009), 336 – 354.

[18] M. Li, T. Tang and B. Fornberg, A compact fourth-order finite difference scheme for the steady incompressible Navier-Stokes equations, *International Journal for Numerical Methods in Fluids* **20** (10) (1995), 1137 – 1151.

[19] S.J. Liao, Higher-order streamfunction-vorticity formulation of 2D steady-state Navier-Stokes equations, *International Journal for Numerical Methods in Fluids* **15** (5) (1992), 595 – 612.

[20] C.H. Marchi, R. Suero and L.K. Araki, The lid-driven square cavity flow: numerical solution with a 1024 × 1024 grid, *Journal of the Brazilian Society of Mechanical Sciences and Engineering* **31** (3) (2009), 186 – 198.

[21] M. Mustafa, T. Hayat, I. Pop and A. Aziz, Unsteady boundary layer flow of a Casson fluid due to an impulsively started moving flat plate, *Heat Transfer – Asian Research* **40** (6) (2011), 563 – 576, DOI: 10.1002/htj.20358.

[22] S. Nadeem, Rizwan Ul Haq and C. Lee, MHD flow of a Casson fluid over an exponentially shrinking sheet, *Scientia Iranica* **19** (6) (2012), 1550 – 1553.

[23] H. Nishida and N. Satofuka, Higher-order solutions of square driven cavity flow using a variable-order multi-grid method, *International Journal for Numerical Methods in Engineering* **34** (2) (1992), 637 – 653.

[24] Y.F. Peng, Y.H. Shiau and R.R. Hwang, Transition in a 2-D lid-driven cavity flow, *Computers & Fluids* **32** (3) (2003), 337 – 352.

[25] M. Sahin and R.G. Owens, A novel fully implicit finite volume method applied to the lid-driven cavity problem – Part I: High Reynolds number flow calculations, *International Journal for Numerical Methods in Fluids* **42** (1) (2003), 57 – 77.

[26] H. Takami and K. Kuwahara, Numerical study of three-dimensional flow within a cubic cavity, *Journal of the Physics Society of Japan* **37** (6) (1974), 1695 – 1698.

[27] D.C. Wan, Y.C. Zhou and G.W. Wei, Numerical solution of incompressible flows by discrete singular convolution, *International Journal for Numerical Methods in Fluids* **38** (8) (2002), 789 – 810.

[28] E. Weinan and J.G. Liu, Vorticity boundary condition and related issues for finite difference schemes, *Journal of Computational Physics* **124** (2) (1996), 368 – 382.